Evaluation quality parameters of DEM generated with low-cost UAV photogrammetry and Structure-from-Motion (SfM) approach for topographic surveying of small areas

***Peter Blistan*[1], *Ľudovít Kovanič*[1], *Matej Patera*[1] *and* *Tomáš Hurčík*[1]**

Conventional geodetic methods and instruments such as total station, or GNSS, are commonly used for geodetic surveying of the ground surface. In recent years, with the development of drones - light Unmanned Aerial Vehicles (UAV) and their combination with a digital camera, opens new opportunities in the field of Earth's surface documentation. This combination of technologies made it possible to use digital photogrammetry to quickly and operatively document the Earth's surface. Using UAV photogrammetry, we can create an accurate and detailed surface model. The surface model can be created as GRID, TIN, respectively as a cloud of points, generated by processing aerial survey images in some processing software, for example, Agisoft Photoscan®. Its accuracy depends essentially on two sets of factors. One group are factors that depend on camera parameters, image flight and LMS processing. The second group consists of factors that influence the accuracy of the model - they depend on the modelling method used and the number of points used to create the terrain model. The research presented in this paper aims to analyze the accuracy of digital elevation models (DEM) created from a various dense cloud of points, obtained using low-cost UAV photogrammetry. The aim was to define - determine the relationship between the number of points entering the modelling and the accuracy of the terrain model obtained from the gradually diluted point-clouds. Quarry Jastrabá in the Slovak Republic was chosen as a representative tested area. The terrain in the quarry has a morphologically indented surface and is thus suitable for verifying the functional dependence between the number of points and the quality - the accuracy of the resulting model. The results show that it is possible to identify the relationship between the number of points used to create a terrain model and the accuracy of the model. This article aims to present the UAV utility for surface documentation and DEM creation. This article addresses the accuracy of the DEM and the optimum amount of points needed to generate it.

Keywords: *UAV, photogrammetry, structure from motion, DEM, point-cloud, GCP, regression analysis, RMSE.*

1. Introduction

During geodetic activities, we often encounter a requirement for surface landscape documentation to create a digital model (DEM). The documentation of the terrain is usually acquired by classical geodetic methods and instruments like GNSS or total stations (TS). In large areas, this process is laborious and slow. As a product of geodetic measurements carried out for documentation of the terrain, a file with X, Y, Z coordinates is obtained (Kovanic et al., 2013). As a result, DEM is usually created and evaluated. Its quality depends directly on the accuracy of the devices and methods used and mainly on the number of measured points. To achieve a precise and detailed surface model, it is necessary to survey more points on the terrain. This process is time-consuming, and nevertheless, we will not achieve the detail and quality of the surface model obtained, for example, terrestrial laser scanning (TLS), LIDAR (Moudry et al., 2019) or photogrammetry approach. Mentioned methods are known as non-selective. Their primary product is the dense point-cloud, which is subsequently processed. For the large ground mapping, mainly the aerial photogrammetry is particularly relevant.

With regard to the obtained results, it is likely the most appropriate equivalent of laser scanning. The current trend in photogrammetry is the use of unmanned aerial vehicles - UAV (Zhang and Elaksher, 2011). UAV photogrammetry is a cheap and in specific conditions accurate method of the surface documentation to create topographic maps and DEM (Colomina and Molina, 2014, Remondino et al., 2011, Neitzel and Klonowski, 2011).

UAV utilization and use of SfM brings benefits in several geosciences. E.g. in mining (Xiang et al., 2018), (Kovanic et al., 2017), (Blistan et al., 2016), (Fraštia et al. 2019), (Frastia, 2005), (Pukanska et al. 2014), (Vegsoova et al. 2019a), (Vegsoova et al. 2019b), potholing (Pukanska et al. 2017), structural geology (Fleming Zachariah et al., 2018), The use of UAVs for steep slope documentation is presented in this work (Agüera-Vega et al., 2018), Monitoring and stability of slopes and landslides (Yu et al., 2018), (Ardi et al., 2018), (Rossi et al., 2018), The accuracy and evaluation of DEM is addressed (Goetz et al., 2018), (Kršák et al., 2016), (Mali et al., 2018), (Polat et al., 2018) or 3D reconstruction techniques and SfM – (Carrivick et al., 2016), (Bartos et al., 2017) etc.

[1] *Peter Blišťan, Ľudovít Kovanič, Matej Patera, Tomáš Hurčík,* Institute of Geodesy, Cartography and GIS, BERG Faculty, Technical University of Kosice, Park Komenského 19, 04384, Kosice, Slovak Republic, *peter.blistan@tuke.sk*

UAVs (Fig. 2) offer simple control using special software - control software (Siebert and Teizer, 2014). It includes the UAV itself, as well as the control centre on the ground (Mozas-Calvache et al., 2012). Working with the UAV, apart from the flight itself, involves many activities (Shahbazi et al., 2015). The mapping workflow consists of the definition of the preparatory phase, the flight planning, the autonomous flight, the quality check of the data and the data processing. It is appropriate to use the GCP for the georeferencing of the model. Determination of coordinates on GCP can be done from the optimized coordinate network (Štroner et al., 2017), where the systematic errors are maximally suppressed (Braun et al., 2015). The final data products are elevation models, orthoimages, 3D models (Eisenbeiss, 2011; Nex and Remondino, 2013). The general workflow for UAV data acquisition and processing is in Figure 3.

Inexpensive UAV carriers are currently available. In terms of price-performance ratio, they are an interesting solution for reducing the incurred costs. Their main drawbacks are inferior quality compact cameras, which are used due to their low weight mainly with cheap and smaller UAV´s. In our research, we focus on verifying the quality of the DEM surface of the quarry obtained by photogrammetry using a low-cost UAV. This problem deals with many works (Fritz et al., 2013; Niranjan et al., 2007; Moudry et al., 2019; Urban et al., 2018). The benefit of this article is the analysis of the quality of the model in terms of the minimum (or optimal) amount of points needed to its generation. We can prove that the precision of the surface model created by low-cost UAVphotogrammetry meets the required accuracy criterion and the models thus obtained should be considerably cheaper, reliable and more detailed than DEM created from points using GNSS or LIDAR.

2. Material and Methods

2.1. Study area

As the area of interest for testing and evaluation of the quality of the DEM obtained by UAV photogrammetry, the quarry site Jastrabá near Žiar nad Hronom in Slovakia was chosen (Figure 1). In this quarry, the excavation of perlite is starting at present. The terrain relief in the quarry is unstable and morphologically rugged. Therefore the standard geodetic measurements are complicated. In the direction of the slope of the terrain, there are numerous furrows formed by flowing water during heavy rainfalls. These furrows are on average 15-20cm deep, but some reach a depth of 50 cm (Figure 1). This terrain is interesting for its complexity and its difficulty documentation using GNSS or TS. The detailed surveying of the entire surface of the quarry with the focus at least the deepest furrows would be time-consuming, and the resulting model would not be able to its true shape capture in necessary detail. Surveying all the smaller terrain features (about 15cm deep) is practically not possible. This quarry was chosen due to the occurrence of different surface types – flat (smooth) and rough.

Fig. 1. Area of interest – quarry Jastrabá

2.2. Methods and equipment

The low-cost UAV DJI Phantom 4 (Fig. 2 and Table 1) was used for the photogrammetric measurement. The flight was conducted in 6 airstrips in height 30 m above the average terrain level (Figure 4). During the flight, 178 images were taken. Longitudinal and lateral image overlap was set to 80%. For the transformation of the frame block into the S-JTSK coordinate system used in the Slovak republic, ten ground control points (GCP) were used. Their coordinates were determined terrestrially by the total station Leica TS 02 using the spatial polar method. Local coordinates were transformed by congruent transformation on connecting points determined by GNSS method. Leica GPS 900 instrument with differential RTN corrections was used. Consequently, the absolute horizontal and vertical RMSE were up to ± 20mm and ±40mm. Relative (inner) spatial RMSE of the GCPs was up to ± 5mm.

Tab. 1. DJI Phantom 4 – technical parameters.

Aircraft	
Weight (Battery & Propellers included):	1380g
Max Ascent / Descent Speed:	6m/s / 4m/s
Max Flight Speed:	20m/s
Max. flight time:	28 min.
Camera	
Operating Environment Temperature:	0℃-40℃
Sensor size:	1/2.3"
Effective Pixels:	12 Megapixels
Focal length	20mm
FOV	94°
Resolution:	4000×3000
Gimbal pitch	-90° to +30°
Remote Control	
Communication Distance (open area):	CE Compliant: 3,5km; FCC Compliant: 5km

Fig. 2. UAV – DJI Phantom 4

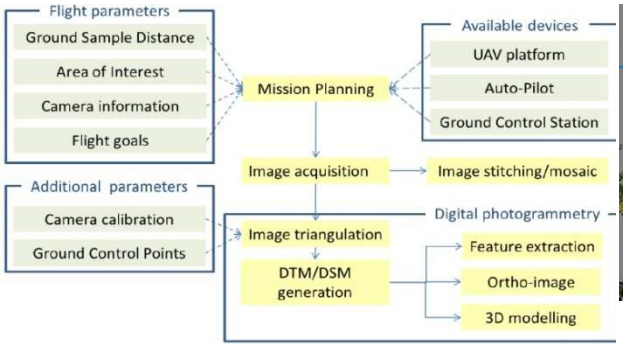

Fig. 3. Workflow for UAV data acquisition and processing (Nex and Remondino, 2013).

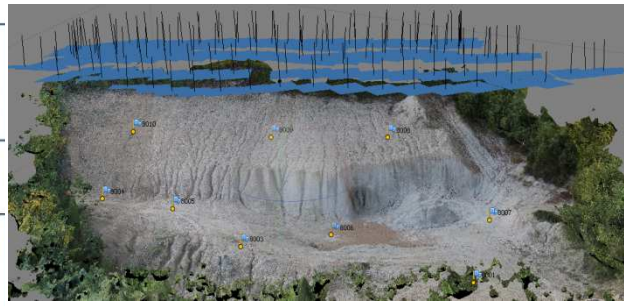

Fig. 4. Terrain model with the position of images and GCP

Processing of the images was performed by the photogrammetric software Agisoft PhotoScan® using the Structure from Motion method. Parameters of image alignment were set to highest with generic preselection of the images. Key point limit value was set to 40000. RMSE value on GCP´s before optimization was 55mm and 33 after the optimization. Value of residuals on control points was 45mm. GSD is 10mm / pixel. Dense cloud generation parameters were set to high quality with mild depth filtering to maintain high detail. In whole locality, 22 million points were generated. While processing, the ground extraction was performed to maintain surface details and the sufficient number of morphology points on the terrain.

Digital elevation model (DEM)

The Digital Elevation Model (DEM) is most often formed by a triangular network generated between directly or indirectly surveyed points, for example, photogrammetric measurement (Chen and Yue, 2010). DEM created from geodetic measurements is usually presented in the form of a wire model with a triangular structure,

and in the case of DEM created from photogrammetric measurements, this wire model is complemented by a photorealistic texture. Using photorealistic texture creates almost perfect digital copies of the real world.

The quality of DEM depends on the density of the input data, the accuracy of the geodetic method used to collect the data, and the selection of the interpolation method used to generate it (Song and Nan, 2009; Hurst, 2014).

Several methods are used to generate DEM. Delaunay triangulation belongs to the simplest ones. Delaunay triangulation as a duality to the Voronoi diagram is based on the definition that each cell of the Voronoi diagram contains one point from the set. The sides of the cell located exactly halfway between the Pi and Pj points of the two adjacent cells represent the axis perpendicular to the triangulation edge, can be seen in Figure 5. In other words, by joining two neighbouring Voronoi cells, we get the Delaunay triangulation edge. In each dimension, intertwined orthogonality applies (George and Borouchaki, 1998).

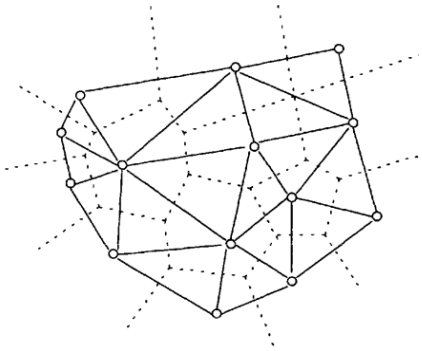

Fig.5. Delaunay triangulation(George and Borouchaki, 1998).

Point clouds preparation

Images obtained by aerial photogrammetry were fully processed by Agisoft PhotoScan®. Obtained dense point-cloud was exported. 3D model of the area of the whole quarry and the nearest surroundings was obtained (Fig. 4). Objects such as vegetation and air points were filtered using ground extraction in Trimble RealWorks® software. Subsequently, the area of interest was cropped by the polygonal fence to create a final selection for further processing. The whole cut out was named as General surface - 1500m^2 with dimensions of approximately 50 x 25m. This area was divided into two smaller parts having different morphometric characteristics. One part was less rugged, flat and was named as Flat (smooth) surface - 700m^2. The second, more rugged area was named Rough surface 350m^2 (Fig. 6). The preparatory work thus resulted in three point-clouds in separated files.

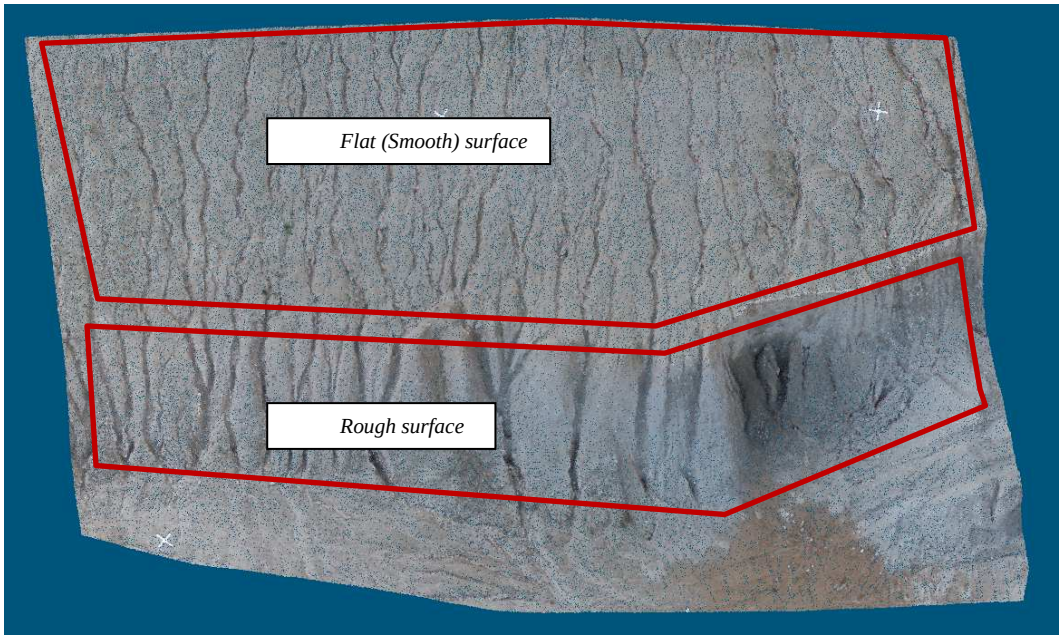

Fig.6. Dividing of the surfaces

The next step was the gradual dilution of point-clouds. The original dense point-clouds were spatially filtered using Trimble RealWorks®. The density of the points was gradually decreased over a range density from 5cm to 100cm. In this range, separate sets were created. Point-clouds with an interval of density dilution of 5 cm were obtained. For a distance between points from 1 m to 5 m, the interval of density dilution was 1 m. Examples of point-clouds are shown in fig. 7. Statistical parameters of generated point-clouds as the number of points per $1m^2$ area for individual areas are shown in Table 2.

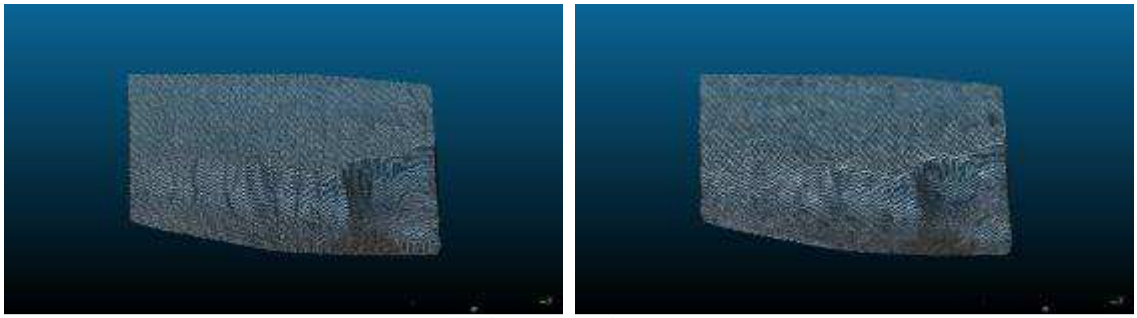

Fig.7. Examples of the spatially filtered point-clouds

The original cloud without spatial filtration was chosen as the reference. Mesh surfaces for these point-clouds were generated. The created models contained 1 218 667 points for the General area, 333 857 points for the Flat part and 473 212 points for the Rough part.

Comparing each set of points with the corresponding reference surface, their distances were determined. The CloudCompare v. 2.10.2 software was used. The shortest distances of each point of the compared set to the local mesh model of the reference surface were determined. The total RMSE of the individual files from the reference model is expressed in Tab. 2.

On fig. 8 (a) to (j), the calculated surface differences for the General area are shown graphically. Because of a large number of files, only selected files corresponding to the distance between points are listed. On fig. a) – 5 cm, b) – 20 cm, c) – 40 cm, d) – 60 cm, e) – 80 cm, f) – 100 cm, g) – 200 cm, h) – 300 cm, i) – 400 cm, j) – 500 cm. Similarly, fig. 9 and fig. 10 shows differences for Flat and Rough surfaces. They are displayed according to the same colour scale. The highest differences are approaching to the red colour.

Tab. 2: Statistics of the point-clouds and calculated parameters

	General surface			*Flat surface*			*Rough surface*		
Distance between points (m)	*Number of points*	*Number of points per 1m²*	*RMSE (m)*	*Number of points*	*Number of points per 1m²*	*RMSE (m)*	*Number of points*	*Number of points per 1m²*	*RMSE (m)*
Dense point-cloud	*1 218 667*	*870*	-	*333 857*	*742*	-	*473 212*	*1121*	-
0,05	*374 587*	*268*	*0,009*	*110 021*	*245*	*0,008*	*136 700*	*324*	*0,011*
0,1	*114 924*	*83*	*0,010*	*34 305*	*77*	*0,008*	*41 353*	*100*	*0,013*
0,15	*55 548*	*40*	*0,012*	*16 951*	*38*	*0,008*	*20 051*	*48*	*0,014*
0,2	*33 138*	*24*	*0,014*	*9 786*	*22*	*0,008*	*11 761*	*28*	*0,014*
0,25	*21 468*	*16*	*0,013*	*6 529*	*15*	*0,009*	*7 691*	*19*	*0,014*
0,3	*15 117*	*11*	*0,013*	*4 663*	*11*	*0,009*	*5 479*	*13*	*0,017*
0,35	*11 381*	*9*	*0,013*	*3 509*	*8*	*0,010*	*4 162*	*10*	*0,018*
0,4	*8 920*	*7*	*0,014*	*2 637*	*6*	*0,010*	*3 154*	*8*	*0,018*
0,45	*7 195*	*6*	*0,016*	*2 118*	*5*	*0,011*	*2 490*	*6*	*0,020*
0,5	*5 700*	*5*	*0,017*	*1 740*	*4*	*0,012*	*2 040*	*5*	*0,023*
0,55	*4 714*	*4*	*0,020*	*1 448*	*4*	*0,013*	*1 687*	*4*	*0,024*
0,6	*3 990*	*3*	*0,021*	*1 239*	*3*	*0,013*	*1 442*	*4*	*0,025*
0,65	*3 442*	*3*	*0,022*	*1 087*	*3*	*0,014*	*1 235*	*3*	*0,028*
0,7	*2 981*	*3*	*0,022*	*949*	*3*	*0,015*	*1 090*	*3*	*0,031*
0,75	*2 607*	*2*	*0,025*	*802*	*2*	*0,015*	*954*	*3*	*0,033*
0,8	*2 320*	*2*	*0,027*	*692*	*2*	*0,016*	*834*	*2*	*0,032*
0,85	*2 089*	*2*	*0,027*	*618*	*2*	*0,018*	*734*	*2*	*0,034*
0,9	*1 903*	*2*	*0,028*	*564*	*2*	*0,018*	*654*	*2*	*0,037*
0,95	*1 669*	*2*	*0,030*	*502*	*2*	*0,019*	*578*	*2*	*0,039*
1	*1 492*	*2*	*0,031*	*464*	*2*	*0,019*	*523*	*2*	*0,044*
2	*383*	*1*	*0,063*	*123*	*1*	*0,023*	*145*	*1*	*0,074*
3	*175*	*1*	*0,112*	*58*	*1*	*0,033*	*69*	*1*	*0,126*
4	*102*	*1*	*0,140*	*35*	*1*	*0,045*	*36*	*1*	*0,168*
5	*66*	*1*	*0,192*	*23*	*1*	*0,058*	*26*	*1*	*0,225*

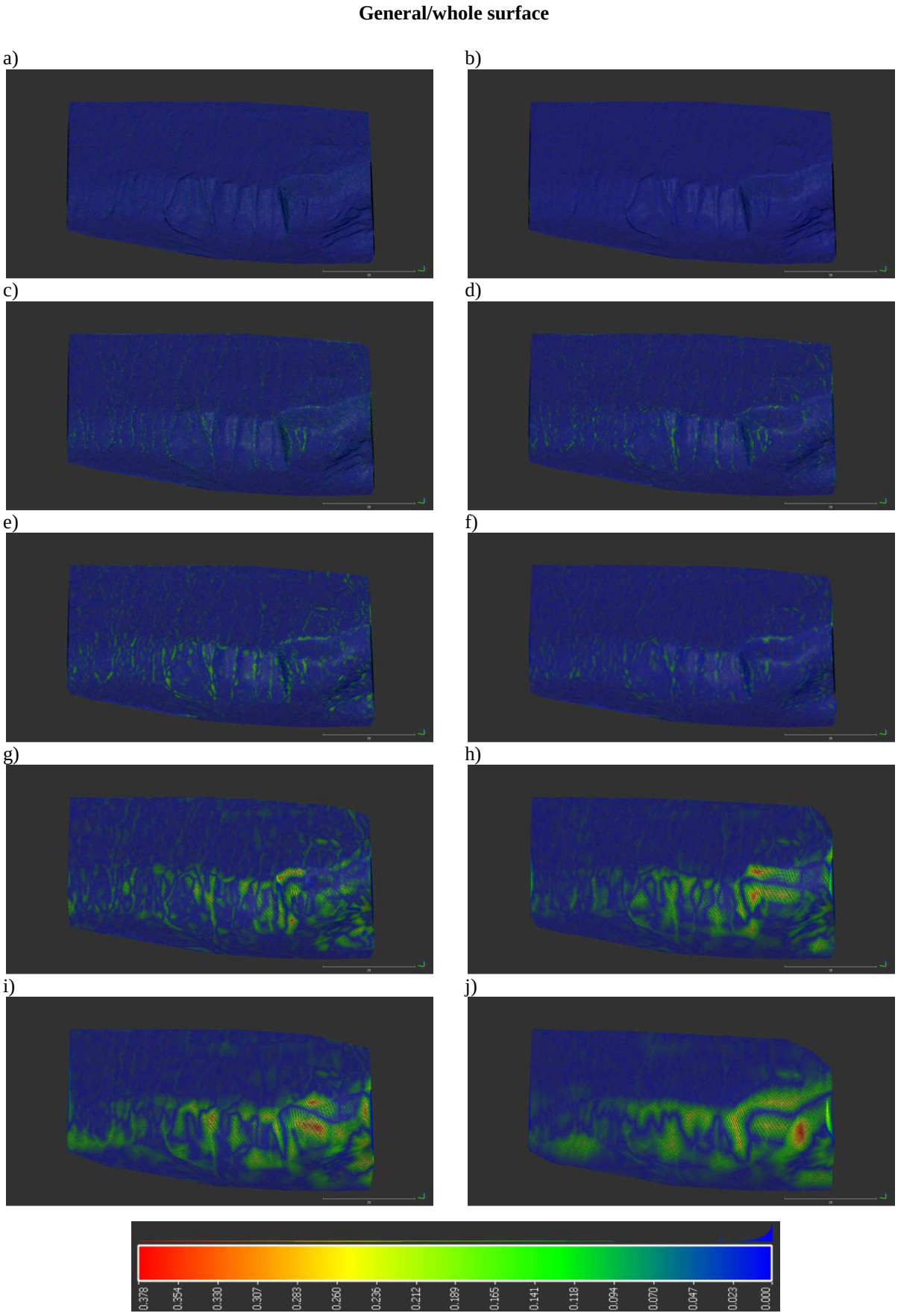

Fig. 8: Differences of the compared point-cloud to the reference model – General surface

Flat/smooth surface

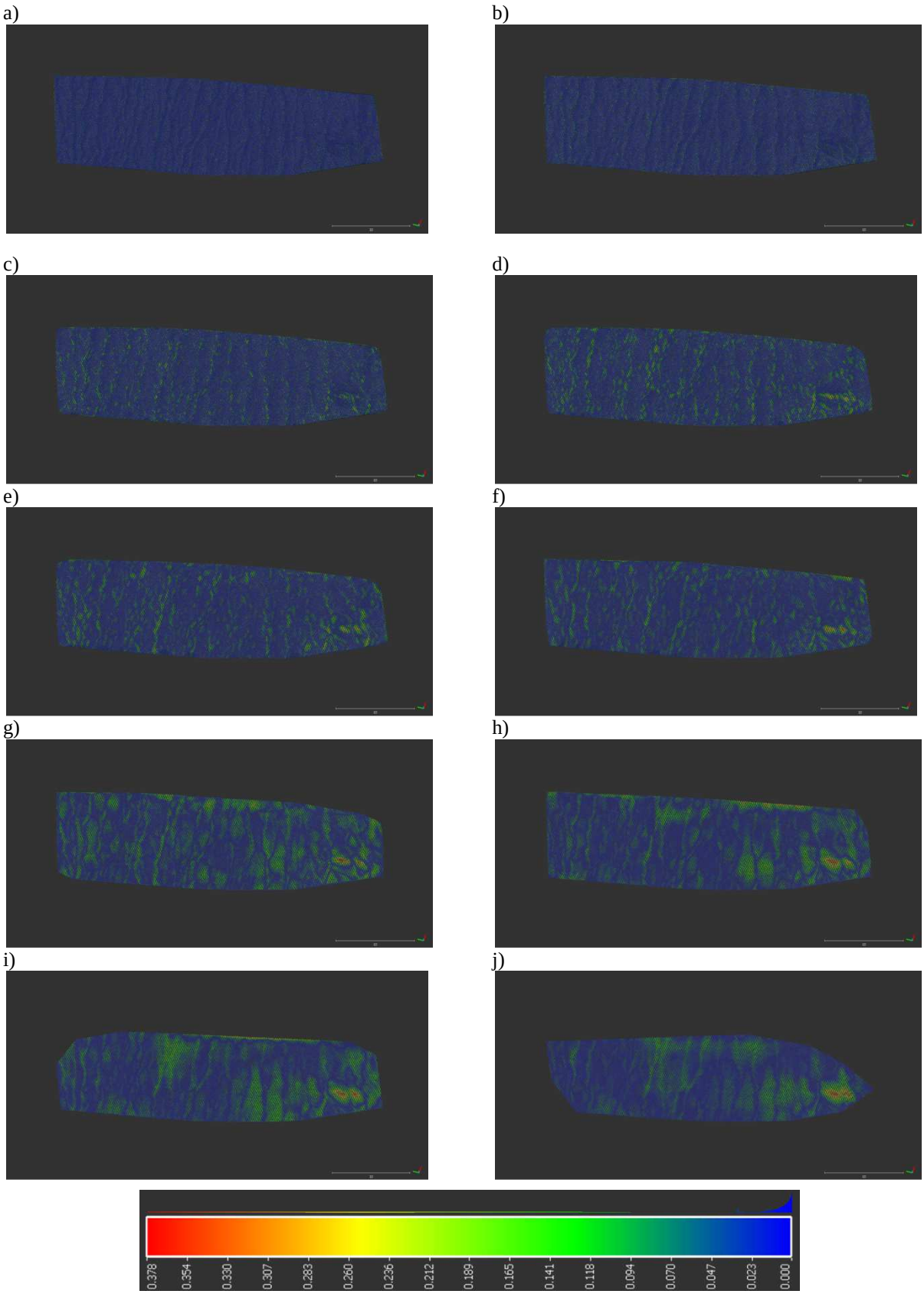

Fig. 9: Differences of the compared point-cloud to the reference model – Flat surface

Rough surface

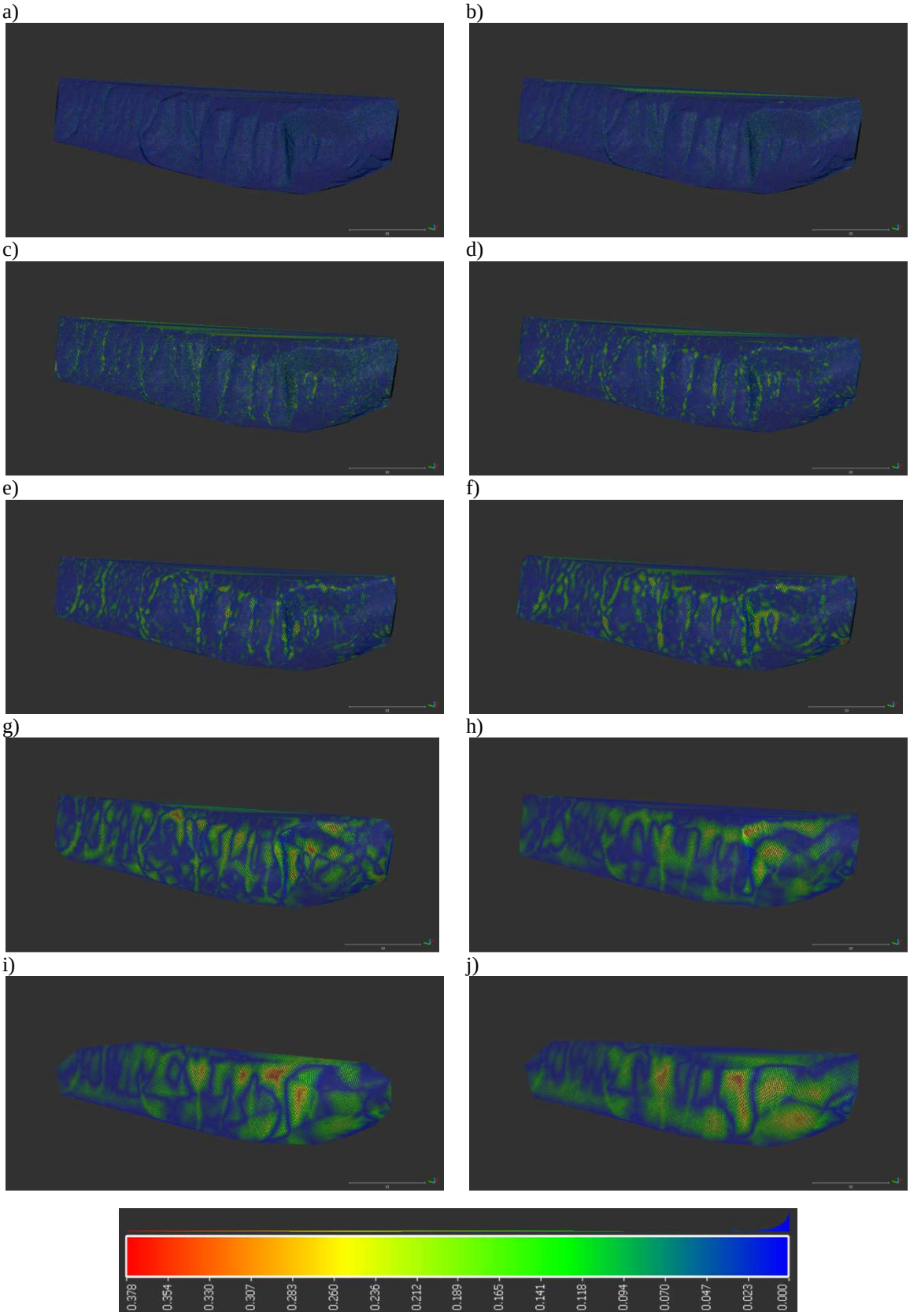

Fig. 10: Differences of the compared point-cloud to the reference model – Rough surface

Results and discussion

Regression and correlation analysis

Several mathematical functions were used during processing. However, polynomial functions have proved to be most suitable for the dependence of point distance and standard deviation and the power function for the point distance and number of points per unit area.

Polynomial function: $f(x) = \alpha + \beta.x + \gamma.y^2 + \delta.x^3 + ...$
Power function: $f(x) = n.x^{-a}$

Functional dependence and the degree of functional dependence for individual surface types were calculated using regression and correlation analysis. A polynomial function preferably approximates the dependency between variables. The regression model equations describe the investigated relationship between point distance (point density) and RMSE. The degree of dependence between the analyzed parameters and the modelled function is described by the Pearson coefficient. Based on the polynomial function, an increasing dependence is described where, with increasing distance between points (gradual dilution of points in the cloud, according to Table 2), the value of the RMSE increases. The RMSE results from the result of comparing two clouds against each other, the original with all points and the gradually diluted clouds. As the distance between the points increases, the standard deviation also increases, and thus the accuracy of the modelled object decreases. The values are shown in Tab. 2.

The correlation coefficient R^2 compares the estimated and actual values and reaches values ranging from 0 to 1. In the case of a value of 1, there is a strong correlation (100%) between the estimated and actual values and vice versa. Concerning the results of the regression and correlation analysis, functions describing the dependence between the above parameters, which were burdened with measurement errors, processing errors and random factors, were determined during measurement and processing. Using the computed values with modelling of the determined functions, the resulting graph can be used to determine the number of points per surface area regarding the required accuracy and character of the measured area. Tab. 3 shows the regression curve equations and calculated correlation coefficients separately for all surfaces and the selected maximum distance between points up to 5m and up to 1m. The graphs also show the values determined in the tab. 2. In the graphs on fig. 11 and 12, these dependencies are indicated as follows (values rise from zero values from left to right):
- General/whole: blue
- Smooth/flat: orange
- Rough/rugged: grey.

Tab. 3: Coefficients of polynomial functions and correlation coefficients obtained by regression and correlation analysis of individual surfaces.

- Distance between points: $x \leq 5$**m**:

Surface	**Regression model**	**Adjusted R^2**
General/whole	$y = 0{,}0026x^2 + 0{,}0241x + 0{,}0058$	$R^2 = 0{,}9964$
Flat/smooth	$y = 0{,}0028x^2 + 0{,}0293x + 0{,}008$	$R^2 = 0{,}9988$
Rough	$y = 0{,}0002x^2 + 0{,}0087x + 0{,}0079$	$R^2 = 0{,}9836$

- Distance between points: $x \leq 1$**m**:

Surface	**Regression model**	**Adjusted R^2**
General/whole	$y = 0{,}0098x^2 + 0{,}0131x + 0{,}0088$	$R^2 = 0{,}9810$
Flat/smooth	$y = 0{,}016x^2 + 0{,}0158x + 0{,}0104$	$R^2 = 0{,}9873$
Rough	$y = 0{,}0053x^2 + 0{,}0075x + 0{,}0069$	$R^2 = 0{,}9905$

Using the same method, the functional relations between the point distance (point density) and the number of points per unit area were determined. The power function best approximates this curve. Results are shown in the tab. 4 and on the graphs on fig. 11 and 12 are shown by the black curve.

Tab. 4: Coefficients of power functions and correlation coefficients obtained by regression and correlation analysis for General surface.

- Distance between points: $x \leq 5$**m**:

Surface	**Regression model**	**Adjusted R^2**
General/whole	$y = 1{,}0425x^{-1{,}869}$	$R^2 = 0{,}9996$

- Distance between points: $x \leq 1$**m**:

Surface	**Regression model**	**Adjusted R^2**
General/whole	$y = 1{,}1129x^{-1{,}865}$	$R^2 = 0{,}9994.$

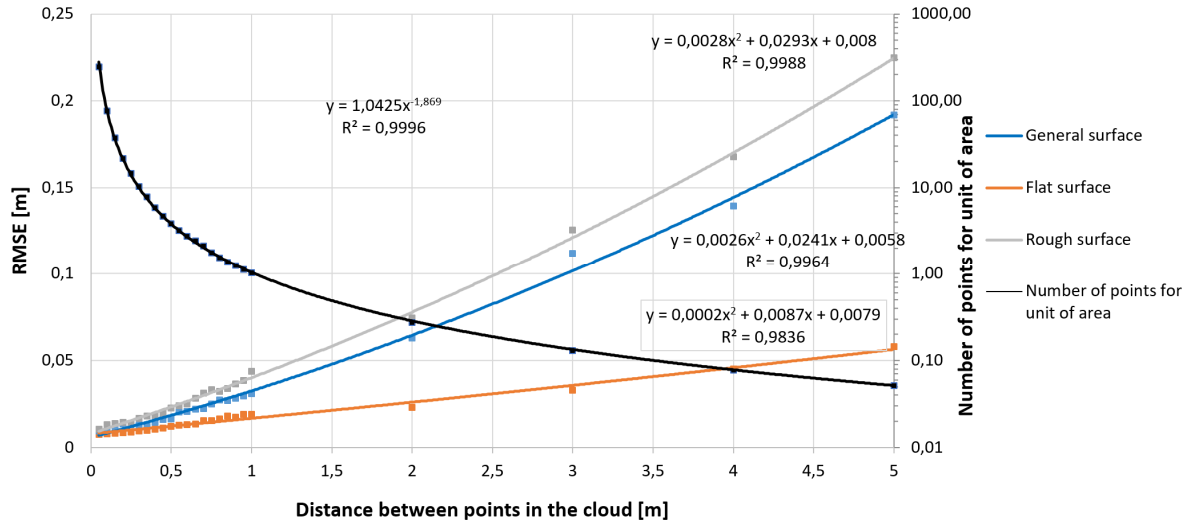

Fig. 11: Graphical representation of regression functions for individual terrain models - a distance of points up to 5m

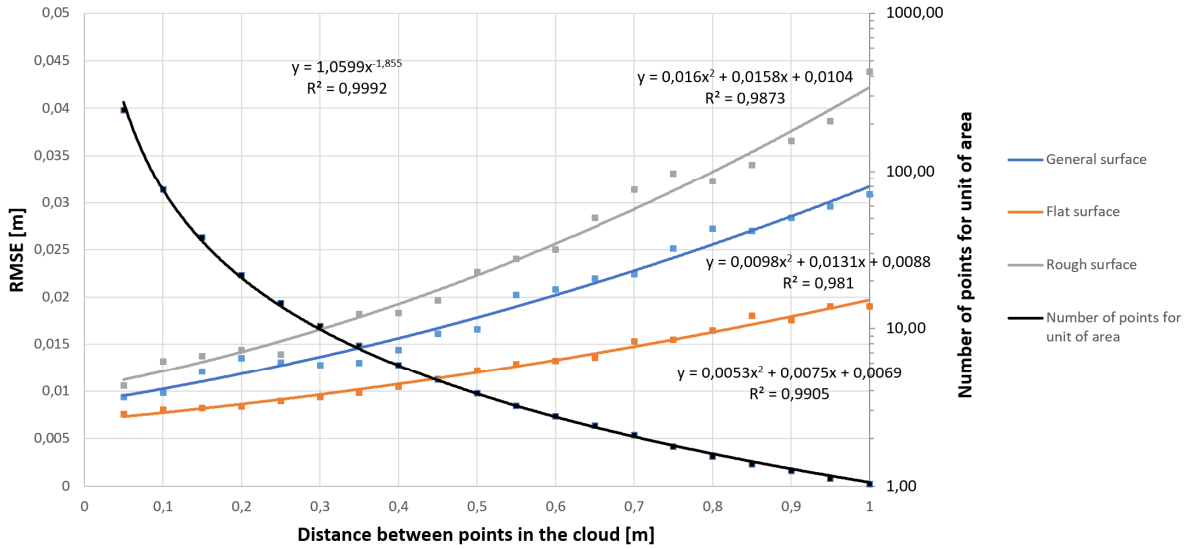

Fig. 12: Graphical representation of regression functions for individual terrain models - a distance of points up to 1m

Based on measured and processed data in the form of evaluation of their functional dependencies, we can obtain two types of functions between three variables (accuracy, the distance between points, number of points per area unit), which are connected by functional links. When solving the accuracy of a model we can determine before measuring how exactly, in terms of the number of points and their distance from each other, we have to survey

the given surface to achieve the necessary modelling accuracy. Such a procedure can be used in practice, for example, in aerial photogrammetry, laser scanning, classical geodetic measurement, where the required density of points in mapping will be determined based on our results.

Analytical solution of the dependence of model quality on the number of points

Fig. 11 and 12 are graphical representations of regression functions expressing the quality of the terrain model as a function of the number of points used to their modelling. The nomograms in Fig. 13 and 14 express the dependence of the accuracy of the terrain model on the amount of input data. In practice, nomograms can be used for:

- determining the minimum number of points per unit area for required model accuracy
- determination of the minimum mutual distance of points for required model accuracy and vice versa
- determination of the standard deviation of the model at a known number of measured points per unit area
- determination of the standard deviation of the model at a known distance between the measured points

Figures 13 and 14 show examples of the use of the nomogram for each model. The colours of the arrows correspond to the colours of the surfaces. Based on the predetermined maximum value of the standard deviation for the design and modelling, we draw a horizontal line from the RMSE scale to the curve of the area under consideration (for example, grey – rough surface). When intersecting the approximation curve of a given surface, the line from the intersection point runs vertically to the scale "Distance between points in the cloud (m)". Finally, we place the horizontal line again from the point of intersection of the power curve (black) to the scale "Points per unit area". In this way, we get an indication of the number of points needed to achieve a given accuracy. Reciprocally, if we know the number of points per unit area in an existing cloud and we assume the type of surface we can determine the expected RMSE. The third way of using the nomogram is if we know the distance of points in the existing cloud as an input parameter. Then it is possible to derive RMSE from the nomogram.

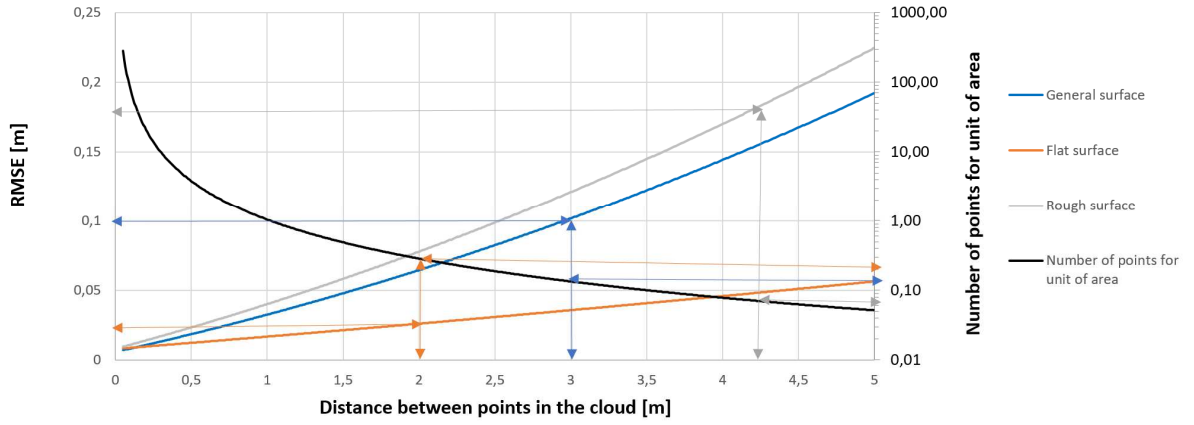

Fig.13: Functional dependence between model quality and number of points used for its creation - a distance of points up to 5m

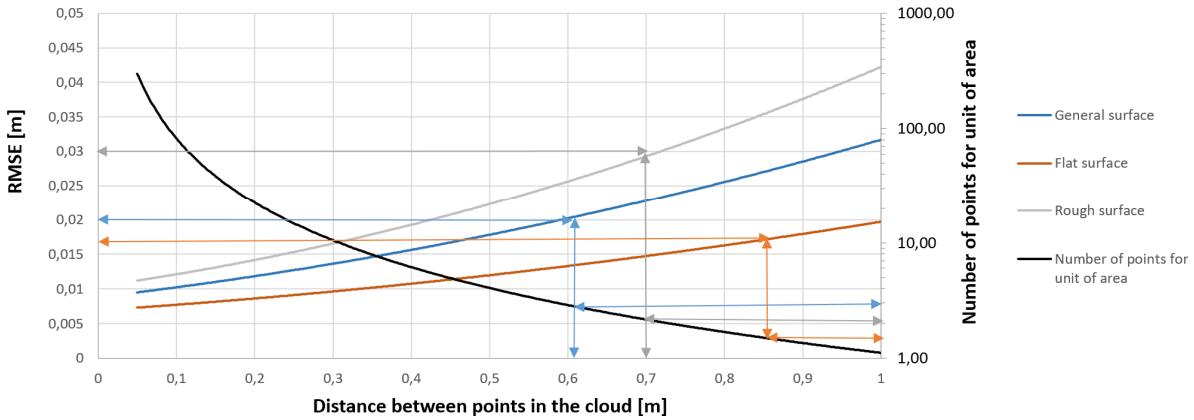

Fig.14: Functional dependence between model quality and number of points used for its creation - a distance of points up to 1m

Conclusion

Using the regression and correlation analysis, the most suitable regression functions for describing the quality of the terrain model at the representative locality Jastrabá estimated. The locality is specific in that it was possible to allocate two types of surfaces - rough and flat. The correlation and regression analysis determines the dependence between the distance of points and the standard deviation expressing the quality of the resulting model. The dependence between the number of points per unit area and the standard deviation expressing the quality of the resulting model was also determined.

Nomograms were created from regression models expressing the functional dependence between the quality of the model and the number of points used for its creation. Nomograms were created for three types of surfaces - rough, flat and general. A nomogram with a mutual distance of points up to 5m can be used for common geodetic measurements using TS or GNSS. The nomogram with the mutual distance of points to 1m can be used for terrestrial or UAV laser scanning or UAV photogrammetry.

Acknowledgement: *This work was supported by project SKHU/1601/4.1/187, by the Scientific Grant Agency of the Slovak Republic (VEGA – MŠVVaŠ SR) through the project. No. 1/0844/18 and the Cultural and Educational Grant Agency of the Slovak Republic (KEGA – MŠVVaŠ SR) through the project. No. 004TUKE-4/2019.*

References

Agüera-Vega, F., Carvajal-Ramírez, F., Martínez-Carricondo, P., Sánchez-Hermosilla López, J., Mesas-Carrascosa, F. J., García-Ferrer, A., & Pérez-Porras, F. J. (2018). Reconstruction of extreme topography from UAV structure from motion photogrammetry. *Measurement: Journal of the International Measurement Confederation, 121*, 127-138. doi:10.1016/j.measurement.2018.02.062

Ardi, N. D., Iryanti, M., Asmoro, C. P., Nurhayati, N., & Agustine, E. (2018). Mapping landslide potential area using fault fracture density analysis on unmanned aerial vehicle (UAV) image. Paper presented at the *IOP Conference Series: Earth and Environmental Science, , 145*(1) doi:10.1088/1755-1315/145/1/012010

Bartos, K., Pukanska, K., Repan, P., Ksenak, L., Sabova, J. (2019) Modelling the Surface of Racing Vessel's Hull by Laser Scanning and Digital Photogrammetry. *REMOTE SENSING*, Vol. 11 (13), DOI: 10.3390/rs11131526

Blistan, P., Kovanič, Ľ., Zelizňaková, V., & Palková, J. (2016). Using UAV photogrammetry to document rock outcrops. *Acta Montanistica Slovaca, 21*(2), 154-161

Braun, J., Štroner, M., Urban, R., & Dvořáček, F. (2015). Suppression of systematic errors of electronic distance meters for measurement of short distances. *Sensors (Switzerland), 15*(8), 19264-19301. doi:10.3390/s150819264

Colomina, I. and Molina, P. (2014) Unmanned aerial systems for photogrammetry and remote sensing: A review, *ISPRS Journal of Photogrammetry and Remote Sensing, Volume 92, Pages 79–97, 2014*.

Eisenbeiss, H. (2011) The Potential of Unmanned Aerial Vehicles for Mapping, Photogrammetrische Woche 2011, Dieter Fritsch (Ed.), Wichmann Verlag, Heidelberg, pp. 135-145

Fraštia, Marek - Liščák, Pavel - Žilka, Andrej - Pauditš, Peter - Bobáľ, Peter - Hronček, Stano - Sipina, Slavomír - Ihring, Pavol - Marčiš, Marián. Mapping of debris flows by the morphometric analysis of DTM: a case study of the Vrátna dolina Valley, Slovakia. In Geografický časopis. Vol. 71, no. 2 (2019), s. 101-120. ISSN 0016-7193

Fraštia, Marek. Possibilities of using inexpensive digital cameras in applications of close-range photogrammetry. In Slovak Journal of Civil Engineering. Vol. 13, No. 2 (2005), s.20-28. ISSN 1210-3896.

Fleming Zachariah, D., & Pavlis Terry, L. (2018). An orientation based correction method for SfM-MVS point clouds—Implications for field geology. *Journal of Structural Geology, 113*, 76-89. doi:10.1016/j.jsg.2018.05.014

Fritz, A., Kattenborn, T. and Koch, B. (2013) UAV-based photogrammetric point clouds - tree stem mapping in open stands in comparison to terrestrial laser scanner point clouds, International Archives of the Photogrammetry, Remote Sensing and Spatial Information Sciences, Volume XL-1/W2, 2013, UAV-g 2013, 4 – 6 September 2013, Rostock, Germany

George, P. and Borouchaki, H. (1998) Delaunay Triangulation and Meshing. Application to Finite Elements. Editions Hermes, Paris, 1998

Goetz, J., Brenning, A., Marcer, M., & Bodin, X. (2018). Modeling the precision of structure-from-motion multi-view stereo digital elevation models from repeated close-range aerial surveys. *Remote Sensing of Environment, 210*, 208-216. doi:10.1016/j.rse.2018.03.013

Hurst, P.J. (2014) A Comparison of Interpolation Methods for Estimating Mountaintop Removal, (2014), Directed by Dr. Rick L. Bunch, pp 86

Chen, C. and Yue, T. (2010) A method of DEM construction and related error analysis. Computers & Geosciences , 36, (2010), pp 717-725

Kovanič, L. (2013). Possibilities of terrestrial laser scanning method in monitoring of shape deformation in mining plants. [Mozliwości wykorzystania naziemnego skaningu laserowego w monitorowaniu deformacji w zakładach górniczych] *Inzynieria Mineralna, 14*(1), 29-41

Kovanič, Ľ., Blišťan, P., Zelizňaková, V., & Palková, J. (2017). *Surveying of open pit mine using low-cost aerial photogrammetry* doi:10.1007/978-3-319-45123-7_9

Kršák, B., Blišťan, P., Pauliková, A., Puškárová, P., Kovanič, L., Palková, J., & Zelizňaková, V. (2016). Use of low-cost UAV photogrammetry to analyze the accuracy of a digital elevation model in a case study. *Measurement: Journal of the International Measurement Confederation, 91*, 276-287. doi:10.1016/j.measurement.2016.05.028

Mali, V. K., & Kuiry, S. N. (2018). Assessing the accuracy of high-resolution topographic data generated using freely available packages based on SfM-MVS approach. *Measurement: Journal of the International Measurement Confederation, 124*, 338-350. doi:10.1016/j.measurement.2018.04.04

Moudry, V., Gdulova, K., Fogl, M., Klapste, P., Urban, R., Komarek, J., Moudra, L., Štroner, M., Bartak, V., Solsky, M. (2019). Comparison of leaf-off and leaf-on combined UAV imagery and airborne LiDAR for assessment of a post-mining site terrain and vegetation structure: Prospects for monitoring hazards and restoration success, *APPLIED GEOGRAPHY*, Vol. 104, 32-41 DOI: 10.1016/j.apgeog.2019.02.002

Moudry, V., Urban, R., Stroner, M., Komarek, J., Broucek, J., Prosek, J. (2019). Comparison of a commercial and home-assembled fixed-wing UAV for terrain mapping of a post-mining site under leaf-off conditions, *INTERNATIONAL JOURNAL OF REMOTE SENSING*,Vol. 40 (2), 555-572, DOI:10.1080/01431161.2018.1516311

Mozas-Calvache, A.T., Pérez-García, J.L., Cardenal-Escarcena, F.J., Mata-Castro, E. and Delgado-García, J. (2012) Method for photogrammetric surveying of archaeological sites with light aerial platforms, Journal of Archaeological Science, Volume 39, Issue 2, February 2012, Pages 521–530

Neitzel, F. and Klonowski, J. (2011) Mobile 3D mapping with a low-cost UAV system.Int. Arch.Photogramm. Remote. Sens. *Spat. Inf. Sci. 38 , 2011, pp. 1–6.*

Nex, F. and Remondino, R. (2013) UAV for 3D mapping applications: A review. Applied Geomatics 6 (1) March 2013, pp.1-15. DOI: 10.1007/s12518-013-0120-x

Niranjan, S., Gupta, G., Sharma, N., Mangal, M. and Singh, V. (2007) Initial efforts toward mission-specific imaging surveys from aerial exploring platforms: UAV, in: Map World Forum, Hyderabad, India, 2007

Polat, N., & Uysal, M. (2018). An experimental analysis of digital elevation models generated with lidar data and UAV photogrammetry. *Journal of the Indian Society of Remote Sensing*, , 1-8. doi:10.1007/s12524-018-0760-8

Pukanská, K., Bartoš, K., & Sabová, J. (2014). Comparison of survey results of the surface quarry spišské tomášovce by the use of photogrammetry and terrestrial laser scanning. *Inzynieria Mineralna, 15*(1), 47-54

Pukanská, K., Bartoš, K., Bella, P., Rákay ml, Š., & Sabová, J. (2017). Comparison of non-contact surveying technologies for modelling underground morphological structures. *Acta Montanistica Slovaca, 22*(3), 246-256

Rossi, G., Tanteri, L., Tofani, V., Vannocci, P., Moretti, S., & Casagli, N. (2018). Multitemporal UAV surveys for landslide mapping and characterization. *Landslides, 15*(5), 1045-1052. doi:10.1007/s10346-018-0978-0–129.

Rusnák, M., Sládek, J., Kidova, A., Lehotský, M. (2018) Template for high-resolution river landscape mapping using UAV technology. *Measurement* 2018, 115.

Rusnak, M., Sladek, J., Pacina, J. and Kidova, A (2019) Monitoring of avulsion channel evolution and river morphology changes using UAV photogrammetry: Case study of the gravel bed Ondava River in Outer Western Carpathians. *AREA*, Volume: 51, Issue: 3, Pages: 549-560

Remondino, F., Barazzetti, L., Nex, F., Scaioni, M. and Sarazzi, D.: UAV photogrammetry for mapping and 3D modeling–current status and future perspectives, in: H. Eisenbeiss, M. Kunz, H. Ingensand (Eds.), Proceedings of the International Conference on Unmanned Aerial Vehicle in Geomatics (UAV-g) *2011, Zurich, Switzerland*.

Siebert, S. and Teizer, J. (2014) Mobile 3D mapping for surveying earthwork projects using an Unmanned Aerial Vehicle (UAV) system, Automation in Construction 41 (2014) 1-14

Shahbazi, M., Sohn, G., Théau, J. and Menard P. (2015) Development and evaluation of a UAV-photogrammetry system for precise 3D environmental modeling; Sensors (Switzerland),Volume 15, Issue 11, 30 October 2015, Pages 27493-27524

Song, R. and Nan, J. (2009) Interactive modeling and visualization of 3D geological bodies, ICCIT 2009 - 4th International Conference on Computer Sciences and Convergence Information Technology, 2009, Article number 5367910, Pages 447-450

Štroner, M., Michal, O., & Urban, R. (2017). Maximal precision increment method utilization for underground geodetic height network optimization. *Acta Montanistica Slovaca, 22*(1), 32-42

Urban, R., Štroner, M., Kremen, T., Braun, J., Moser, M. (2018). A novel approach to estimate systematic and random error of terrain derived from UAVs: a case study from a post-mining site *ACTA MONTANISTICA SLOVACA*, Vol. 23 (3), 325-336

Urban, R., Štroner, M., Blistan, P., Kovanič, Ľ., Patera, M., Jacko, S., Ďuriška, I., Kelemen, M. and Szabo, S.: The Suitability of UAS for Mass Movement Monitoring Caused by Torrential Rainfall-A Study on the Talus Cones in the Alpine Terrain in High Tatras, Slovakia. In: *ISPRS International journal of geo-information*. Nr. 8, vol. 8 (2019), pp. 317-317

Vegsoova, O., Straka, M. and Sulovec, M. (2019 a) Global Assessment of Industrial Expansion for Minimizing Environmental Impacts Utilizing the Principles of Mining and Logistics, *Rocznik Ochrona Środowiska*, 21, pp. 14- 28,

Vegsoova, O., Straka, M. and Rosova, A. (2019 b): Protecting and securing an environment affected by industrial activity for future utilization, *Rocznik Ochrona Środowiska*, 21, pp. 98- 111,

Xiang, J., Chen, J., Sofia, G., Tian, Y., & Tarolli, P. (2018). Open-pit mine geomorphic changes analysis using multi-temporal UAV survey. *Environmental Earth Sciences, 77*(6) doi:10.1007/s12665-018-7383-9

Yu, J., Gan, Z., Zhong, L., & Deng, L. (2018). Research and practice of UAV remote sensing in the monitoring and management of construction projects in riparian areas. Paper presented at the *International Archives of the Photogrammetry, Remote Sensing and Spatial Information Sciences - ISPRS Archives, , 42*(3) 2161-2165. doi:10.5194/isprs-archives-XLII-3-2161-2018

Zhang, C. and Elaksher, A. (2011) An unmanned aerial vehicle-based imaging system for 3D measurement of unpaved road surface distresses, J. Comput. Aided Civ.Infrastruct. Eng. 27 (2) (2011) 118